A reevaluation of irregular joint shear behavior on the basis of 3D modelling of their morphology - Part II: Joint Shear Behavior Mechanical Modelling

Guy Archambault, Sylvie Gentier, Joëlle Riss, Rock Flamand, Colette Sirieix

ARCHAMBAULT G., GENTIER S., RISS J. et FLAMAND R.

A reevaluation of irregular joint shear behavior on the basis of 3D modelling of their morphology - Part II: Joint Shear Behavior Mechanical Modelling.

Proc. Second International Conference on Mechanics of Jointed and Faulted Rock (H.P. Rossmanith ed.) 1995, Balkema, pp. 163-68.

A re-evaluation of irregular joint shear behavior on the basis of 3D modelling of their morphology
Part II: Joint mechanical shear behavior and modelling.

Guy Archambault[1], Sylvie Gentier[2], Joelle Riss[3], Rock Flamand[1] & Colette Sirieix[4]

[1]*Centre d'études sur les ressources minérales, Université du Québec à Chicoutimi, Québec, Canada G7H 2B1*
[2]*BRGM, Direction de la recherche, BP 6009, 45060 Orléans Cedex 02, France*
[3]*Centre de développement des géosciences appliquées, Université de Bordeaux I, 33405 Talence Cedex, France*
[4]*ANTEA, Direction de la géotechnique, BP 6119, 45061 Orléans Cedex 02, France*

ABSTRACT: This second part of the paper presents the results of an experimental study on the shear behavior of unfilled natural rock joint replicas in order to consider a renewed approach based on the 3D angular distribution of asperities on the joint mean plane, the 3D surface roughness and the progressive degradation of asperities in relation to the shear displacement and applied normal stress.

1 INTRODUCTION

Literature on rock joint mechanical behavior and their applications to various workings stability analysis is quite abundant over the last fifteen years. The ISRM Commission on Rock Joints organized three symposium on various aspects of this problem (Stephansson, 1985; Barton & Stephansson, 1990; Goodman & Myer, 1992). Few works account for joint surface asperity angularities in the evaluation of the rock joint shear strength and their stress-strain-dilatancy behavior. Even fewer works have been dedicated to the progressive degradation of the joint surfaces during shear displacement.

Regarding the geometrical description of the joint surfaces morphology needed to evaluate the joint shear parameters necessary to model their mechanical behavior, Part I of this paper proposed a 3D statistical description of their morphology: 3D angularity colatitudes (θ_3) and surface roughness (R_A) of asperities structure on the joint surfaces derived from 2D basic data: heights and profiles. It also shows how the 2D morphological characteristics give apparent colatitudes and a biased characterization of the joint wall surfaces as pointed out previously (Riss & Gentier, 1990). These affect greatly the shear behavior modelling of joints.

This second part of the paper is mainly concerned with the results of an experimental study on the shear behavior of unfilled clean rock joint replicas in order to consider an approach based on this 3D statistical description of the joint surfaces morphology. The progressive degradation of asperities on the wall surfaces was also evaluated in relation with shear displacement and applied normal stress on the joint mean plane.

2 EXPERIMENTAL TESTING AND PROCEDURE

Identical replicas molded from the original sample of a fracture in the Guéret Granite (France), drilled perpendicular to the fracture plane, were used in this study. The characterization of this fracture surface morphology has been studied in detail (Gentier, 1987; Riss & Gentier 1989, 1990) and also in Part 1. Molds of both walls were made by casting them with a silicon elastomer and these molds were used to create the replicas. The material used was a non-shrinking mortar with the following characteristics: σ_c = 82 MPa, σ_t = -6,6 MPa, E = 32 200 MPa and the basic friction angle is ϕ_b = 37°. Each replica was adjusted carefully in a steel box, to ensure that all replicas were in the same position. The samples have a circular section with a shear surface of 90 mm in diameter.

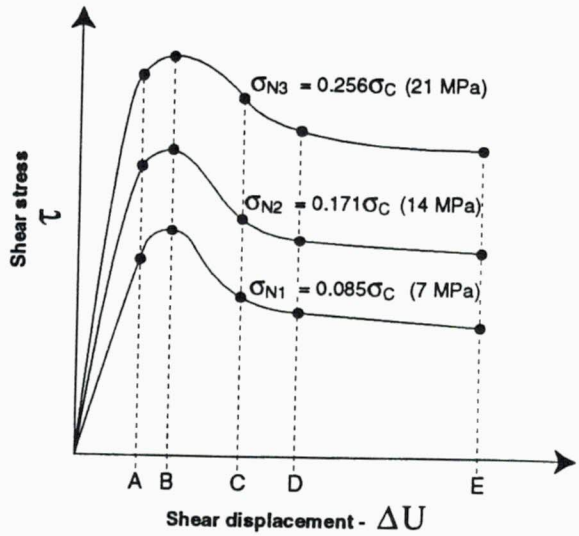

Figure 1. Direct shear test program

A series of direct shear tests were performed for five different shear displacement (ΔU) under three different normal stress (σ_N) applied on the shear plane. Each shear test was stopped at a defined shear displacement, illustrated by the black dots in figure 1, and a new replica was used for each one. So, this procedure permits a better control on the evolution of the joint wall surfaces morphology with shear displacement. The applied normal stresses on the shear plane were 7, 14 and 21 MPa. Shear displacements were interrupted for each applied normal stress in the following sequence: before the peak strength (ΔU at A), another test at peak strength (ΔU at B), two tests were interrupted between the peak and residual shear strengths (ΔU at C and D), and finally another test was conducted up to residual strength (ΔU at E). These shear displacements were the following: 0,35 mm (for A), 0,55 mm (for B), 1,0, 2,0 and 5,0 mm (for C, D and E).

The direct shear test program was realized at the BRGM research division laboratory in Orléans, France. The shear machine device used was designed and built at the BRGM and is equiped with data acquisition and servo-control systems. The latter system permits direct shear tests to be performed under constant normal stress conditions by decreasing the normal force proportionally to the reduction in shear surface during the test. It also allows variable shear displacement rate testing. In this study, the shear rate used was 0,5 mm/min. Markers on the samples and tightening wedges inside the shear boxes controlled the shear direction from test to test and avoided a change in shear direction during direct shear tests. At the end of each test (the shear stress, shear displacement, normal stress and normal displacement being available), a morphological analysis was performed using profiles z = f(x,y) recorded on the joint wall surfaces as detailed in Part 1 of the paper.

When adjusted together, the corresponding profiles of both walls show the contact areas and void spaces between these walls (Fig. 2). It is clear from this figure that the applied normal stress on the shear plane was redistributed on a small portion of the total area. Also, it may be observed that the contact area are mostly on the slopes of the asperities.

For the first time, simultaneous mechanical shear test results and surface characteristics of the morphology evolution for various shear displacements, are available in an overall data set. All the data are of the same nature obtained from identical replicas of a natural fracture used for the experimental shear tests.

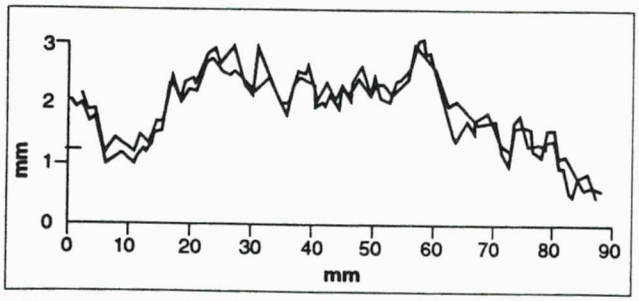

Figure 2. Example of contact areas and void spaces in the studied fracture along profile 3.

3 DIRECT SHEAR TEST RESULTS AND DISCUSSION

The direct shear test results: shear stress (τ) - shear displacement (ΔU) and dilatancy (ΔV) - shear displacement (ΔU) curves are shown in figure 3 for the three constant normal stress loading conditions imposed on the specimens: σ_{N1} = 7 MPa (0,085 σ_c), σ_{N2} = 14 MPa (0,171 σ_c) and σ_{N3} = 21 MPa (0,256 σ_c) and for the five shear displacements studied at each normal stress level.

The principal observations on the behavior of the shear stress-displacement characteristics at failure and residual phases are summarized in Tables 1 and 2. The parameters are σ_N, the applied normal stress; $\overline{\tau}_f$, the mean peak shear strength; τ_R, the residual shear strength; $\Delta\overline{U}_f$, the mean peak shear displacement and $d\overline{n}_f°$, the peak dilation angle.

Table 1. Direct shear tests results.

σ_N (MPa)	$\overline{\tau}_f$ (MPa)	τ_R (MPa)	$\Delta\overline{U}_f$ (mm)
7	10,90	6,24	0,41
14	18,78	12,10	0,53
21	24,23	17,00	0,61

Table 2. Peak dilation angles.

σ_N (MPa)	$d\overline{n}_f°$ (degrees)
7	14,1
14	11,7
21	10,4

The peak shear displacement occurred rapidly, between 0,41 and 0,61 mm. The shear stress-shear displacement curves (Fig. 3) show a pre-peak linear elastic mobilization of the shear stress, under friction condition, accompanied by a closure on the joint plane followed by a non-linear shear stress-shear displacement hardening caused by the dilatancy mobilization to peak shear strength under a nearly constant peak displacement model (Goodman, 1976) in relation with the normal stress magnitude. The post-peak phase show a progressive softening due to a progressive degradation of the joint surfaces with a decreasing shear stress to residual shear strength (Fig. 3). This last phase is almost reached between 3,0 and 5,0 mm of shear displacement but the degradation of the joint surfaces is still operating at the end by ploughing, friction and wear processes on the joint plane asperities and by particles comminution on it.

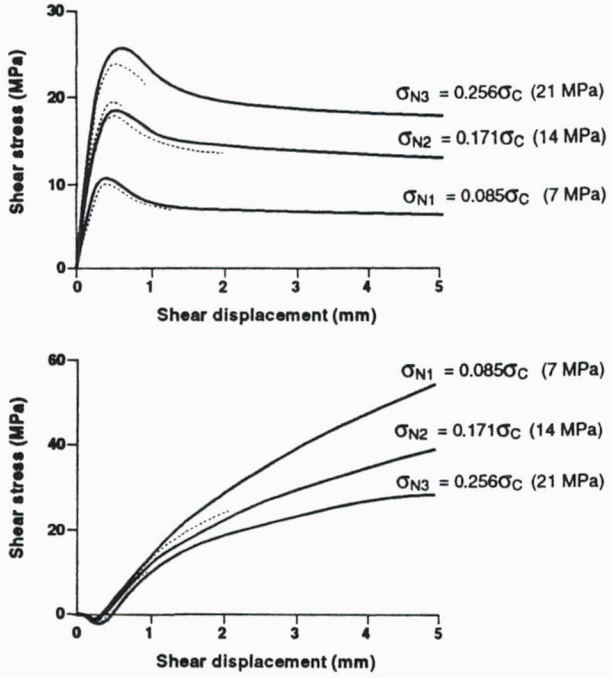

Figure 3. Direct shear test results under σ_{N1}=7 MPa) ; σ_{N2} =14 MPa) and σ_{N3} =21 MPa) conditions and for five replicas at each normal stress

The dilatancy curves (Fig. 3) show, for the same normal stress (five replicas tested at each normal stress), a first phase of contractancy (negative dilatancy) from 0,00 and 0,25 mm of shear displacement adding to the previous one (not shown) caused by the applied normal stress on the joint shear plane well evaluated by Gentier (1987). This last closure phase result from an adjustment or a consolidation with the application of the shear stress causing a better matching between the two joint surfaces. From 0,25 mm of shear displacement, dilatancy by overriding of asperities are mobilized at a high rate or angle to peak shear displacement; followed by a decreasing rate with post-peak shear displacement, for a given normal stress. It trends progressively towards zero for large shear displacement under low normal stress, but for smaller displacement under higher normal stress (Fig. 3). Increasing normal stress decreased the rate of dilatancy both at peak and for post-peak shear displacement (Table 2 and Fig. 4).

The direct shear test results are plotted on a Mohr diagram (Fig. 4) in which the triangles represent the values of $\overline{\tau}_f$ for σ_N = 7, 14 and 21 MPa (Table 1). The dotted line indicate the shear tests results performed on saw-cut surfaces in mortar blocks for the same normal stress values. A basic friction angle ϕ_b = 37° was evaluated from these tests. Other points correspond to the ultimate shear strength measured at ΔU = 2, 3,5 and 5 mm respectively. In the bottom diagram (Fig. 4) are plotted the corresponding dilatancy rate (or angle) for the three normal stress values studied both at peak shear strength and at ultimate shear strength for 5 mm shear displacement.

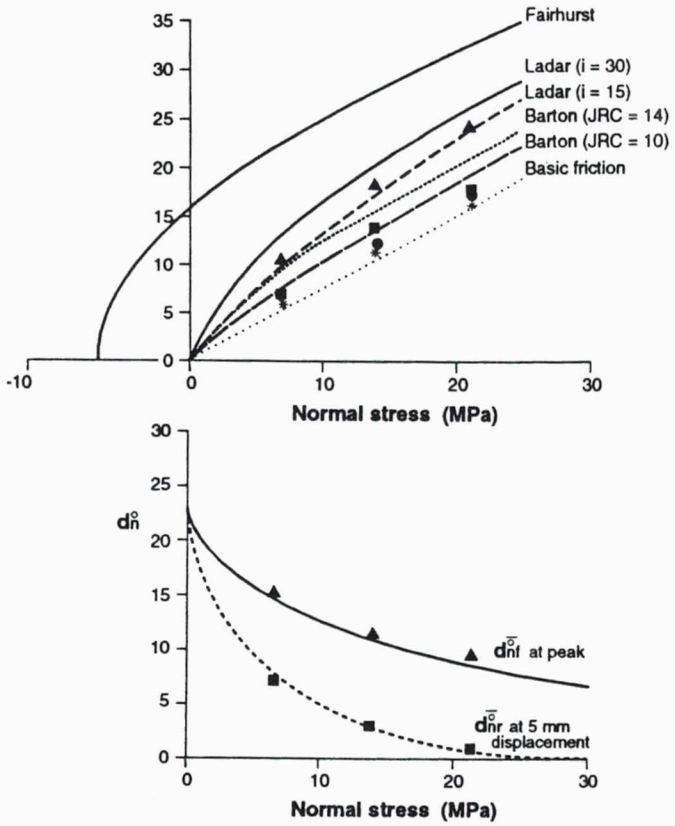

Figure 4. Calculated peak strength envelopes and dilatancy variation with normal stress according to models and test results.

The thick line (Fig. 4, upper part) is the intact rock material shear strength calculated with Fairhurst's failure criteria. The thin and long-dashed lines represent the predicted τ_f values with the LADAR model (Ladanyi & Archambault, 1969) for i_0 = 15° and i_0 = 30° respectively. Values of τ_f were calculated with Barton's model (Barton, 1973) for JRC = 10 and JRC = 14 evaluated for the replicas surface morphology.

It can be seen that, for both JRC values, the shear strength predicted by Barton's model tends toward residual shear strength as σ_N increase. For low normal stress level σ_{N1} = 0,085 σ_c (7 MPa), the predicted τ_f is significantly lower than the value obtained from the corresponding shear test and the discrepancies increase with increasing normal stress.

τ_f values calculated with the LADAR model, for initial asperity angles i_0 = 15° and i_0 = 30°, resulted in a better agreement with peak shear strength results with an i_0 value around 16° to 17°. The direct shear test results trend toward the intact material shear strength failure envelope, as predicted by the LADAR model behavior, with increasing normal stress.

In addition to the roughness profiles, the progressive degradation of the asperities and the evolution of contact areas were studied with digitized black and white photographs (figure 5). On these photographs, black pixels correspond to the dammaged portions of the surface. For the three photographs, σ_N was at 14

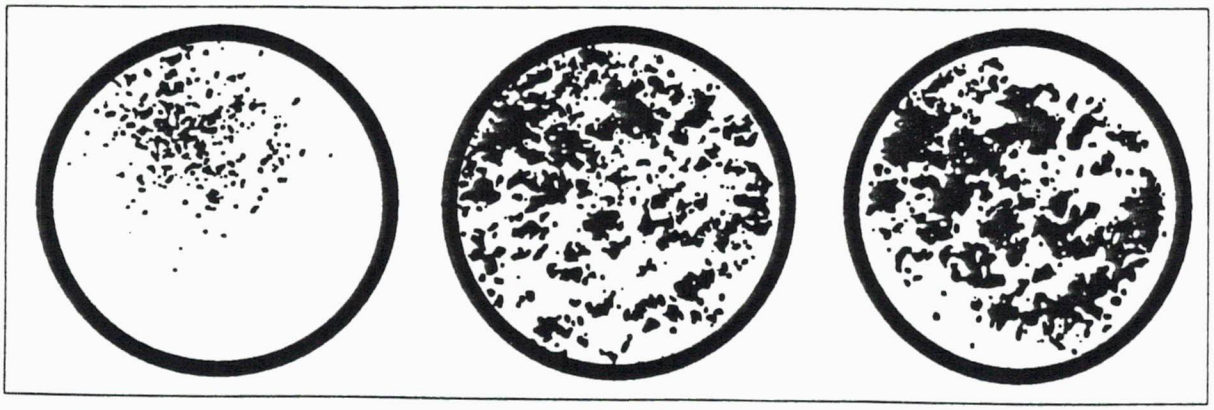

Figure 5. Progressive surface degradation with shear displacement for σ_{N2}=14 MPa. Black pixels represent damaged portions

MPa and the chosen replica is pink colored for a better contrast between intact and damaged areas. Figure 5a and 5b show the sheared areas at τ_f ($\Delta U_B \cong$ 0,55 mm) and τ ($\Delta U_D \cong$ 2,0 mm) respectively and finally, figure 5c shows the damaged portions at τ_R ($\Delta U_E \cong$ 5,0 mm). These figures demonstrate clearly that the asperity degradation depends not only on the magnitude of the normal stress, but mainly on the shear displacement after peak shear strength at which degradation is very light at low normal stress.

The proportion of contact areas on the sample's surfaces is quite small in regards with the total area of the sample (Gentier, 1987; and figure 2). Thus, the normal stress on the contact areas are much higher than the mean applied normal stress on the samples. Despite this fact, for the three relatively low applied normal stresses, very few asperities were sheared off at peak shear strength (ΔU_B). Thus, it may be assumed that for low σ_N, most of the resisting shear force comes from friction on the sliding areas and from the work done by dilatancy against the normal stress. But for higher σ_N values, an increasing proportion of asperities failure must be taken into account in a failure component which must be part of the shear-dilatancy model.

The resulting dilation angle at the peak shear strength evaluated from the direct shear tests range from 14,1° to 10,4° with increasing σ_N (Table 2), while the 2D asperity angles computed from five linear roughness profiles in the shear direction on intact samples, provide mean values of θ_2 around 10° (Part I). These are positive angles mobilized during a shear test. This means that, even for low or median normal stress, dilatancy angles show higher values than asperities angularity distribution evaluated on the intact samples 2D profiles. This is confirmed by the closer relationship with the LADAR model indicating asperity angles around 15°. Thus, 2D profiles underestimate the true angularity of asperities in giving an apparent dip angle. The reason is that profiles rarely passed through the summit of asperities (or true dip) as demonstrated in Part I and underlined in previous papers (Riss & Gentier, 1989 and 1990). As proposed previously (in Part I), this bias may be corrected by an analysis which restore the 3D colatitudes θ_3 distribution of elementary plane facets of the asperities composing the joint wall surfaces. This correction permits to evaluate the true angularity of the asperities giving new 3D angularities distribution with a mean around 16° and a mode around 13° (Fig. 6) more in agreement with experimental observations on dilatancy angles behavior during the shear tests on the joint replicas under low normal stress conditions and with the i_0 values indicated by the LADAR model.

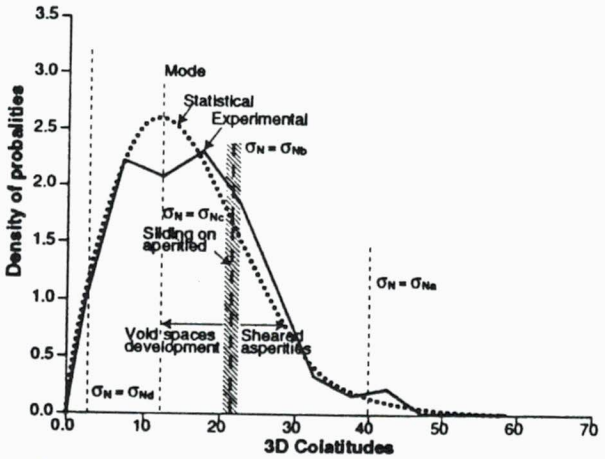

Figure 6. Reconstructed 3D distribution of tested fracture replicas integrating both walls asperities distributions and showing various normal stresses effects on the asperities distribution in relation with shear behavior

Decreasing $\overline{d n_f}°$ values were observed with increasing σ_N (Fig. 3 & 4). Thus, for low σ_N values applied on the joint plane, high angles of asperity (θ_3) are mobilized in friction, resulting in a higher rate of dilatancy, lower shear strength, limited areas of contact and surface degradation at peak, accompanied by the development of greater void spaces. At higher normal stresses, lower angles of asperity (θ_3) are mobilized in friction, while the asperities showing higher angularities are sheared off. This results in an

increase τ_f with two components operating simultaneously: friction on inclined area of contacts and failure of asperities with higher angularity under mode I or II or both. Increasing areas of contact and degradation, as well as lower rates (or angles) of dilatancy and void spaces development will be observed on the joint shear surfaces at peak. This is well illustrated in figure 6 in relation with the 3D colatitudes distribution of asperities (or true angularity) for a given σ_N value.

4 IMPLICATIONS ON ROCK JOINT SHEAR MODELLING

A compilation of peak dilation angles and τ/σ_N values measured during shear tests on rock joints in various rock type by different workers (Barton, 1973), Barton's own results as well as those from Ladanyi & Archambault (1980) on irregular tensile fracture and many others in the last decade show for most of their results a certain trend for i_0 values varying between 15° and 35°. The first are for high normal stress while the latters correspond to low normal stress, which is oftenly the case in experimental literature on the subject matter. It is surely why the failure component of asperities was neglected in most of the proposed models even in Rowe et al. (1964) stress-dilatancy model where it was assumed that there was no breaking of soil grains or of the conceptual spheres on which the model was developed but only sliding on them.

The shear process of a joint with irregular surfaces may be summarized in the following scenario: application of the normal load concentrates the normal stress on very few points (contact areas) , as pointed out previously, with a simultaneous closure on the joint depending on the normal load magnitude, well discussed in the literature. It is followed by the shear load application giving rise to a transfer of the stresses on the asperities slopes defined by their angularity, in these area. This shear force application result in a new closure on the joint with an increasing contact areas and a linear elastic mobilization of the shear stress on the inclined plane of the asperities. It is followed by a non-linear shear stress/shear displacement hardening phase resulting from the mobilization of dilatancy on the joint plane to peak shear strength. Asperities within a restricted domain of angularity, in these contact area, are mobilized in friction on the irregular joint plane, which dictates the rate of dilatancy in a shear stress/shear displacement/dilatancy process on the joint shear plane. Asperities with higher angularity than the range of the mobilized angularities are immediately sheared off for very small shear displacement and are showing frictional behavior thereafter; while asperities with lower angularity are creating voids by separation of the two surfaces of the joint in these areas and the increase in void spaces depend on the rate of dilatancy (Fig. 6). On the other hand, for lower normal stress values ($\sigma_N = \sigma_{Na}$, Fig. 6) applied on the joint plane, high slope angles of asperities are mobilized in friction resulting in higher rate of dilatancy, lower shear strength, limited areas of contact and degradation on irregular joint surfaces and greater void spaces. At higher normal stress ($\sigma_N = \sigma_{Nb}$ or σ_{Nc}, Fig. 6), lower angles of asperity are mobilized in friction resulting in increasing shear strength, areas of contact and degradation as well as lower rate of dilatancy and void spaces creation are observed. Finally, at very high applied normal stress ($\sigma_N > \sigma_{Nd}$, Fig. 6) on the joint plane, near the brittle-ductile transition pressure, most of the asperities are sheared off and the shear behavior of the joint is nearly similar to intact rock material at this stress level.

5 CONCLUSION

In the modelling approach, the 3D colatitudes (θ_3) must be used to characterize asperities angles on the irregular joint surface instead of the usual 2D characterization with linear roughness profiles. Also, the modelling must integrate these characteristics in the usual stress (shear and normal)/shear displacement/dilatancy model for peak shear strength taking into account simultaneous sliding on a mobilized asperities angularity and failure for higher asperity angularities. The shear behavior modelling or shear stress/normal stress/shear displacement/normal displacement relationships must also integrate the degradation process on the joint wall surfaces as a function of the normal stress magnitude and shear displacement. Equally, these relationships must deal with the fundamental shear process on irregular joint surfaces, in which contact areas on the surface are limited and dependent on the normal stress magnitude in the pre-peak loading phase where the stresses are highly concentrated on these reduced areas. In the post-peak degradation phase of the joint surfaces the contact surface increases progressively as to release the stresses concentration, to reach finally a large surface of contact in the residual strength phase, as a function of shear displacement, where degradation is still operating by ploughing, wear and grinding of the particles on the joint shear plane to produce gauge material.

ACKNOWLEDGEMENT

This is a BRGM contribution nº 94059; this work was financially supported by a BRGM research project, an NSERC of Canada research grant and an NSERC graduate student followship.

REFERENCES

Barton, N. 1973. Review of a new shear-strength criterion for rock joints. *Eng. Geol.* 7: 287-332.

Barton, N. & Stephansson, O. (Eds.) 1990. Rock Joints. Proc. of the International Symposium on Rock Joints, Loen, Norway, June 4-6.

Gentier, S. 1987. Morphologie et comportement hydromécanique d'une fracture naturelle dans le granite sous contrainte normale; étude expérimentale et théorique. Documents du BRGM nº 134, BRGM, Orléans, France, 597 p.

Goodman, R.E. 1976. Methods of Geological Engineering. West Publishing Co. 472 p.

Goodman, R.E. & Myer, L. (Eds.) 1992. Fractured and Jointed Rock Masses. Conference of ISRM Commission on Rock Joints, Lake Tahoe, California, June 3-5.

Ladanyi, B. & Archambault, G. 1980. Direct and indirect determination of shear strength of rock mass. AIME Annual Meeting, Las Vegas, Preprint Nº80-25, 16 p.

Ladanyi, B. & Archambault, G. 1969. Simulation of shear behavior of a jointed rock mass. Rock mechanics - Theory and practive, Proc. 11th Symp. on Roch Mech., California: 105-205.

Riss, J. & Gentier, S. 1989. Linear and areal roughness of non planar rock surfaces of fracture. *Acta Steorol* 8: 677-682.

Riss, J. & Gentier, S. 1990. Angularity of a natural fracture. Proc. Int. Conf. on Mech. of Jointed and Faulted Rock, Rossmanith P. (Ed.), Balkema, pp. 399-406.

Rowe, P.W., Barden, I. & Lee, I.K. 1964. Energy components during the triaxial cell and direct shear tests. *Geotechnique,* 14(3): 247-261.

Stephansson, O. (Ed.) 1985. Fundamentals of Rock Joints. Proc. of the International Symposium on Fundamentals of Rock Joints, Björkliden, Sweden, September 15-20.